Single-cell analyses reveal functional classification of dendritic cells and their potential roles in inflammatory disease

Qian Shi,* Fei Zhuang,* Ji-Ting Liu,* Na Li,* Yuan-Xiu Chen,* Xian-Bin Su,[†] Ai-Hong Yao,[‡] Qing-Ping Yao,* Yue Han,* Shan-Shan Li,* Ying-Xin Qi,*,[1] and Zong-Lai Jiang*

*Institute of Mechanobiology and Medical Engineering, School of Life Sciences and Biotechnology, and [†]Key Laboratory of Systems Biomedicine, Shanghai Center for Systems Biomedicine, Shanghai Jiao Tong University, Shanghai, China; and [‡]College of Computer Science and Technology, Harbin Engineering University, Harbin, China

ABSTRACT: Dendritic cells (DCs) have crucial roles in immune-related diseases. However, it is difficult to explore DCs because of their rareness and heterogeneity. Although previous studies had been performed to detect the phenotypic characteristics of DC populations, the functional diversity has been ignored. Using a combination of flow cytometry, single-cell quantitative PCR, and bioinformatic analysis, we depicted the DC panorama with not only phenotypic but also functional markers. Functional classification of DCs in mouse lymphoid tissue (spleen) and nonlymphoid tissue (liver) was performed. The results revealed that expression of macrophage scavenger receptor 1 (*MSR1*) and C–C motif chemokine receptors (*CCR*)*1*, *CCR2*, and *CCR4* were elevated in liver DCs, suggesting increased lipid uptake and migration abilities. The enriched expression of costimulatory molecule *CD80*, *TLR9*, and TLR adaptor *MYD88* in spleen DCs indicated a more-mature phenotype, enhanced pathogen recognition, and T-cell stimulation abilities. Furthermore, we compared DCs in the atherosclerotic mouse models with healthy controls. In addition to the quantitative increase in DCs in the liver and spleen of the apolipoprotein E–knockout ($ApoE^{-/-}$) mice, the functional expression patterns of the DCs also changed at the single-cell level. These results promote our understanding of the participation of DCs in inflammatory diseases and have potential applications in DC clinical assessment.—Shi, Q., Zhuang, F., Liu, J.-T., Li, N., Chen, Y.-X., Su, X.-B., Yao, A.-H., Yao, Q.-P., Han, Y., Li, S.-S., Qi, Y.-X., Jiang, Z.-L. Single-cell analyses reveal functional classification of dendritic cells and their potential roles in inflammatory disease. FASEB J. 33, 000–000 (2019). www.fasebj.org

KEY WORDS: functional heterogeneity · single-cell qPCR · antigen-presenting cell · atherosclerotic mouse models

Dendritic cells (DCs) were first discovered by Steinman *et al.* (1) in the late 1970s and were named according to their unique tree-like morphology. DCs are broadly distributed in both lymphoid tissues, including the spleen and lymph nodes, and nonlymphoid tissues, such as the liver, lung, dermis, intestine, and aorta (2, 3). Despite their scarce abundance, DCs act as the most potent, professional antigen-presenting cells, capturing, processing, and presenting various exogenous and endogenous antigens to T cells (4). In that way, DCs provide an important link between the innate and adaptive systems.

Increasing evidence has revealed the heterogeneous characteristics of DC populations. DCs are generally subdivided into conventional DCs (cDCs) and plasmacytoid DCs (pDCs) across tissues and species, and a special subset of DCs called epidermal Langerhans cells (LCs) are identified in skin (2). Several surface markers, including CD4, CD8, CD103, and CD11b, have been widely used to further subdivide DCs (5, 6), which exhibit distinct roles in the processes of immune-related diseases. During malarial infection, both splenic CD8$^+$ and CD8$^-$ DCs present malarial peptides and induce IFN-γ production by CD4 T cells, but only CD8$^-$ DCs from infected mice can induce T-cell proliferation (7). In house dust mite–induced asthma, CD11b$^+$ DCs, but not CD103$^+$ DCs, induce T

helper 2 cell responses in lung (8). Intestinal CD103^{+}CD11b^{−} DCs, but not CD103^{+}CD11b^{+} DCs, restrain colitis by triggering a reversible early anti-inflammatory response in epithelial cells *via* proteins induced by IFN-γ, creating an anti-inflammatory environment (9). These studies were generally performed with flow cytometry or immunofluorescence, which cannot provide enough targets for characterizing the heterogeneous and functional diversity of DCs.

In the steady state and in inflammatory diseases, DC subsets express distinct levels of function-related molecules and thus display a series of functional properties (10), including those related to maturation (11), migration (12), oxidized LDL (oxLDL) engulfment (13), adhesion (14), and T-cell stimulation (15). In the steady state, the DCs in nonlymphoid tissues display an immature phenotype with low levels of the costimulatory molecules CD40, CD80, and CD86 (16). After up-regulation of chemokine receptors, such as CCR7, DCs migrate from nonlymphoid tissues *via* the afferent lymph to the draining lymph nodes where they up-regulate expressions of costimulatory molecules and display mature phenotypes (17). DCs can uptake oxLDL *via* scavenger receptors (SRs), such as LOX-1, CD36, and CD205, and this process may lead to aggravation of vascular inflammation (18). The TLR adapter MyD88 of DCs has been reported to be required for the T-cell response in inflammatory bowel disease (19). All of these studies suggest that it is quite necessary to identify the heterogeneity of DCs based on a series of functional markers. Most recently, single-cell analyses (20) have been used to identify heterogeneous populations, and massively parallel RNA single-cell sequencing has provided a new way to explore DC phenotypic heterogeneity (21). However, the important functional changes of DCs were ignored in the massive information of RNA-seq. Compared with single-cell sequencing, single-cell quantitative PCR (sc-qPCR) has advantages of DC classification based on not only phenotypic but also functional markers and shows potential value in clinical application at an economical price with more-easily commercialized target genes.

To demonstrate the functional diversity of DCs, 48 genes were selected in the present study, illustrating the classic phenotype as well as 8 groups of important functional markers of DCs. By a combination of fluorescence-activated cell sorting (FACS) and sc-qPCR, the expression profiles of 48 genes in single DCs from the mouse liver and spleen were detected and then analyzed *via* bioinformatic methods. Furthermore, the functional heterogeneity of single DCs was also compared between a healthy and an atherosclerotic mouse model. The present analyses may provide a new method for functionally discriminating of DC heterogeneity and may expand the understanding of the phenotypic and functional divergence of DCs in different tissues and different diseases.

MATERIALS AND METHODS

Mice

C57BL/6, C57BL/6J and apolipoprotein E–knockout ($ApoE^{−/−}$) mice were obtained from Vital River Laboratory (Beijing, China). All mice were male. The mice were maintained under specific pathogen–free conditions and were fed with a normal diet in the Animal Research Committee facility of Shanghai Jiao Tong University. To establish the atherosclerotic model and the control group, $ApoE^{−/−}$ mice and C57BL/6J mice were fed a high-fat diet or normal chow, respectively, for 12 wk beginning at 8 wk old. Oil-red O (Sangon Biotech, Shanghai, China) staining of the mouse aortae was used to validate the atherosclerosis. All studies were performed in accordance with the principles of the Basel Declaration and recommendations of the *Guide for the Care and Use of Laboratory Animals* (National Institutes of Health, Bethesda, MD, USA) (22). The protocol was approved by the Animal Research Committee of Shanghai Jiao Tong University.

Preparation of the single-cell suspensions

The spleens and livers were isolated from the mice. The tissues were flushed with PBS and excised into small pieces. The mouse spleens were ground and passed through a cell strainer. Next, ACK buffer (ammonium–chloride–potassium; Beyotime, Shanghai, China) was used to remove the red blood cells from the spleen suspensions. The liver cells were prepared following a previously published method (23). The mouse livers were incubated with 770 U/mg collagenase type IV in HBSS containing 10% fetal bovine serum for 1 h at 37°C with gentle shaking. The liver suspensions were then run through a Ficoll 1.077 (GE Healthcare, Waukesha, WI, USA) centrifugation at room temperature to enrich the hematopoietic cells. The spleen suspensions and enriched liver suspensions were kept on ice for the flow cytometry analyses.

Flow cytometry and single-cell sorting

The Fc receptors were blocked before fluorescent labeling. The antibodies used in this study included the following: anti-mouse CD11c-PE (clone HL3; BD Biosciences, San Jose, CA, USA) and anti-mouse MHCII–APC (clone AF6-120.1; BD Biosciences). The samples were analyzed with a FACS Aria II machine (BD Biosciences). The flow cytometry data were analyzed with FlowJo software (Tree Star, Ashland, OR, USA). Individual cells were sorted directly into 96-well PCR plates that were preloaded with 5 µl PCR mix in each well [5 µl CellsDirect 2× reaction mix; Thermo Fisher Scientific, Waltham, MA, USA; 0.1 µl (2 U) Superase-In RNase Inhibitor; Thermo Fisher Scientific]. The plates were immediately put on dry ice and stored at −80°C.

Primer design for the target genes

Forty-eight target genes, including housekeeping genes and DC definition-related, phenotypic, and functional markers, were selected. These genes have distinct molecular functions and participate in a host of biologic processes. The mRNA sequences were downloaded from National Center for Biotechnology Information (Bethesda, MD, USA; *https://www.ncbi.nlm.nih.gov/*), and the primers were designed with Primer 3 software (Thermo Fisher Scientific) (Supplemental Table S1). Next, the primers provided by Sangon Biotech (*http://www.sangon.com/*) were synthesized. The specificities and linearities of those primers were carefully validated before use. The validation experiments were performed to measure the single-cell PCR sensitivity (Supplemental Fig. S1).

Single-cell–specific target amplification

Forty-eight pairs of primers were pooled to a final concentration of 200 nM for each primer. After a brief centrifugation at 4°C, each

well of a 96-well plate was supplemented with 0.2 μl SuperScript III RT-PCR System with Platinum Taq Mix (Thermo Fisher Scientific), 2.5 μl of the mixture of the 48 pooled primers, and 1.3 μl of nuclease-free water (Thermo Fisher Scientific). The plates were then placed on a PCR machine (Bio-Rad Laboratories, Hercules, CA, USA) and incubated for 90 s at 70°C to denature the single cells. The mRNA of each cell lysate was reverse transcribed into cDNA (50°C for 15 min). Then, the reverse transcription was inactivated, and Taq polymerase was activated (95°C for 2 min). Subsequently, preamplification of the specific target was performed in the same tube for 22 PCR cycles (each cycle: 95°C for 15 s and 60°C for 4 min). Finally, a cleanup step was used to remove the unincorporated primers with exonuclease I (New England BioLabs, Ipswich, MA, USA).

High-throughput real-time PCR on a real-time PCR reader

The amplified cDNA from each single cell was diluted 1:5 with nuclease-free water. The diluted samples for the 48 assays were loaded into a M48 chip (Fluidigm, South San Francisco, CA, USA) with an IFC Controller HX (Fluidigm) with EvaGreen DNA Binding Dye (Bio-Rad Laboratories). Then, the chip was transferred to a Biomark real-time PCR reader (Fluidigm). All steps were performed in strict accordance with the manufacturer's protocols and instructions.

Computational analysis of the single-cell data

The single-cell data were analyzed and displayed with the Singular Analysis Toolset (Bell Laboratories, Madison, WI, USA) of the R software (R Foundation for Statistical Computing, Vienna, Austria). The background value was set to 28. Because DCs were commonly defined as lineage (LIN) (CD3, CD19, NK1.1)$^-$CD45$^+$CD11c$^+$MHCII$^+$ cells (24), the sorted single CD11c$^+$MHCII$^+$ DCs by flow cytometry were further quantified with sc-qPCR *via* a series of genes, including the lineage-restricted marker genes (*CD3*, *CD19*, and *KLRB1C*), leukocyte common marker gene *PTPRC* (CD45), and the commonly used DCs marker genes *ITGAX* (CD11c) and *H2-AA* (MHCII). T, B, and NK cells were recognized by the expression of *CD3*, *CD19*, and *KLRB1C* (NK1.1) and were removed from the data set. The cells with no expression of *CD45*, *CD11c*, and *MHCII* were identified as non-DCs and excluded from the data set. The cells with no or low housekeeping gene expression levels were also removed from the analysis. Hierarchical clustering (HC) analysis was used to connect the data points to form clusters based on distance and to help build a binary tree in the form of a heat map. Forty-eight genes were clustered by the Pearson method, and the single DCs from the different mouse tissues were clustered by the Euclidean method (25). Principal component analysis (PCA), a dimension-reduction analysis, was used to simplify the multidimensional data sets from the sc-qPCR experiment for plotting purposes. Forty-eight genes were transformed into 2 principal components. A radar map was drawn to provide an overall concept of the expression differences. The mean values of each of the genes were separately calculated for the liver and spleen DCs and then converted into log$_2$-fold changes. Violin plots were used to display the gene characteristics of burst size and frequency. Some of the genes had unimodal distributions, and others had bimodal distributions.

Immunofluorescence staining

The spleens, livers, and hearts from healthy mice and atherosclerotic model mice were flushed with PBS and fixed with 4% paraformaldehyde. Frozen sections of the mouse livers, spleens, and aorta roots were cut at a thickness of 6 μm using a cryosection technique. The slides were permeabilized with 0.3% Triton X-100 (MilliporeSigma, Burlington, MA, USA). CD11c and CCR7 were stained with biotin-labeled anti-CD11c (clone N418; BioLegend, San Diego, CA, USA) and anti-CCR7 antibody (clone Y59; Abcam, Cambridge, MA, USA), respectively, and detected with an Alexa Fluor 555 Tyramide SuperBoost kit (Thermo Fisher Scientific) and an Alexa-Fluor-488 Anti-Rabbit IgG Kit (Cell Signaling Technology, Danvers, MA, USA), respectively. The nuclei were stained using DAPI (Cell Signaling Technology). Images of the stained sections were collected with a TCS SP8 STED ×3 confocal microscope (Leica, Wetzlar, Germany).

RESULTS

Genes for phenotypic and functional classification of single DCs

To identify the phenotypic and functional classification of single DCs, 48 target genes, divided into the following 4

TABLE 1. *Forty eight Genes for phenotypic and functional classification of single DCs*

Group	Class	Gene
Housekeeping genes	Housekeeping genes	*GAPDH, ACTB*
DC definition-related markers	Lineage restricted genes	*CD3, CD19, KLRB1C, PTPRC*
	Makers of DCs	*ITGAX, H2-AA, H2-K1*
	Makers of macrophages	*FCGR1, MERTK, CD68, ADGRE1*
	Ontogeny markers of DCs	*C-KIT, FLT3, CSF1R*
Phenotypic markers	Reported phenotype genes	*LY6C, BST2, XCR1, SIRPA, CD4, CD8, ITGAE, ITGAM, DC-SIGN, CD207*
Functional markers	Costimulatory molecules	*CD40, CD80, CD86*
	Adhesion molecules	*ICAM1, ICAM2, CDH1*
	TLR	*TLR3, TLR7, TLR9*
	TLR adaptor molecule	*MYD88*
	Scavenger receptors	*OLR1, MSR1, LY75*
	Mannose receptor	*MRC1*
	Chemokine receptors	*CCR1, CCR2, CCR4, CCR7, CCL17, CX3CR1*
	Cytokines	*IL-10, IL-12*

groups, were selected (**Table 1** and Supplemental Table S1): *1*) housekeeping genes, *2*) DC definition-related, *3*) phenotypic, and *4*) functional markers.

GAPDH and *ACTB* were selected as the housekeeping genes. The DC definition-related markers included lineage-restricted marker genes *CD3*, *CD19*, and *KLRB1C* to exclude T, B, and NK cells; *PTPRC* (CD45) as a leukocyte common marker (24); *FCGR1* and *MERTK* to distinguish macrophages from DCs (6); the commonly used DCs markers *ITGAX* (CD11c) and *H2-AA* (MHCII) (24); and *C-KIT*, *FLT3*, and *CSF1R* to track the ontogeny of the DCs (26). Regarding the phenotypic markers, classic marker genes, such as *BST2*, *CD4*, and *ITGAE*, were selected (5, 6). For the functional markers, the following groups of genes were chosen: the costimulatory molecule genes *CD40*, *CD80*, and *CD86* were used to assess the maturation states of the DCs (11); *ICAM1*, *ICAM2*, and *CDH1* were used to indicate the adhesion capacities of the DCs (14); *TLR3*, *TLR7*, and *TLR9* were TLR genes used to aid in the recognition of the nucleic acids of pathogens and self-nucleic acids in disease (27); *MYD88* was selected because the TLR adaptor MYD88 can activate CD4^{+} T cells (15); the scavenger receptor genes *OLR1*, macrophage scavenger receptor 1 (*MSR1*), and *LY75*, as major receptors of oxLDL, were selected for their participation in lipid engulfment

(13); *MRC1*, which encodes the mannose receptor, was chosen for antigen recognition (28); the chemokine receptor genes *CCR1*, *CCR2*, and *CCR7* were chosen for their potential roles in the migration of DCs and T-cell recruitment (12); and genes of the inflammatory cytokines *IL-10* and *IL-12* were also included in the panel to reflect the activation of DCs (29).

Gene profiling of single DCs from spleen and liver

Single DCs isolated from the liver, as a representative nonlymphoid tissue, and the spleen, as a representative lymphoid tissue, were classified based on those 48 phenotypic and functional genes (**Fig. 1**).

Single DCs from cell suspensions of mouse livers or spleens were analyzed with flow cytometry. DCs are generally identified by both CD11c and MHCII (30). In the flow cytometry experiment (**Fig. 2***A*), forward scatter (FSC)-A and side scatter (SSC)-A of light were used to segregate live lymphocytes. Then, singlets from the live lymphocytes were gated by FSC-A and FSC-W. Singlets were further subdivided by CD11c and MHCII. Our flow cytometry data revealed that the percentage of

Figure 1. Workflow of the functional classification of DCs based on single-cell technologies. Single-cell suspensions were isolated from the liver and spleen of C57BL/6 mice. Next, single liver and spleen DCs (CD11c⁺MHCII⁺) were sorted into 96-well plates by FACS. The 48 target genes were divided into the following 4 groups: *1*) housekeeping genes and *2*) DC definition-related, *3*) phenotype, and *4*) functional markers. The sc-qPCR results were used for the bioinformatic analyses and functional classification of the DCs.
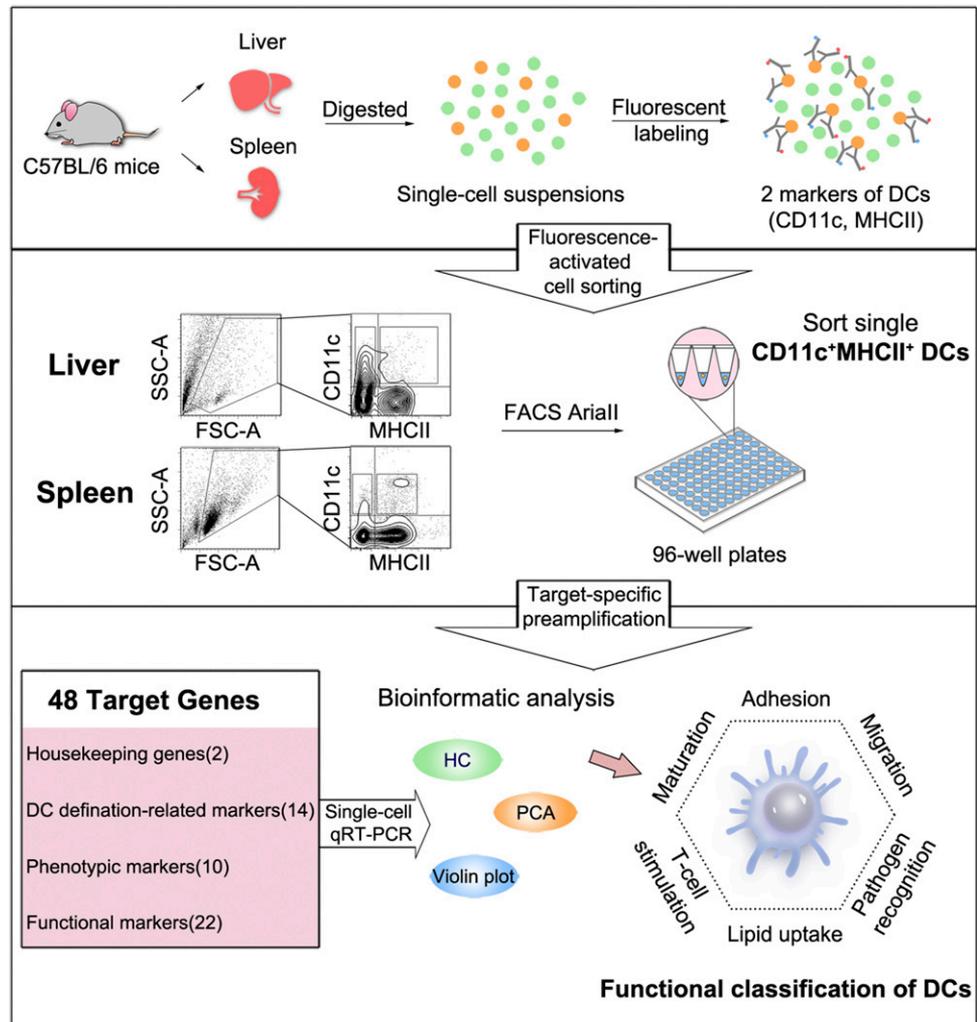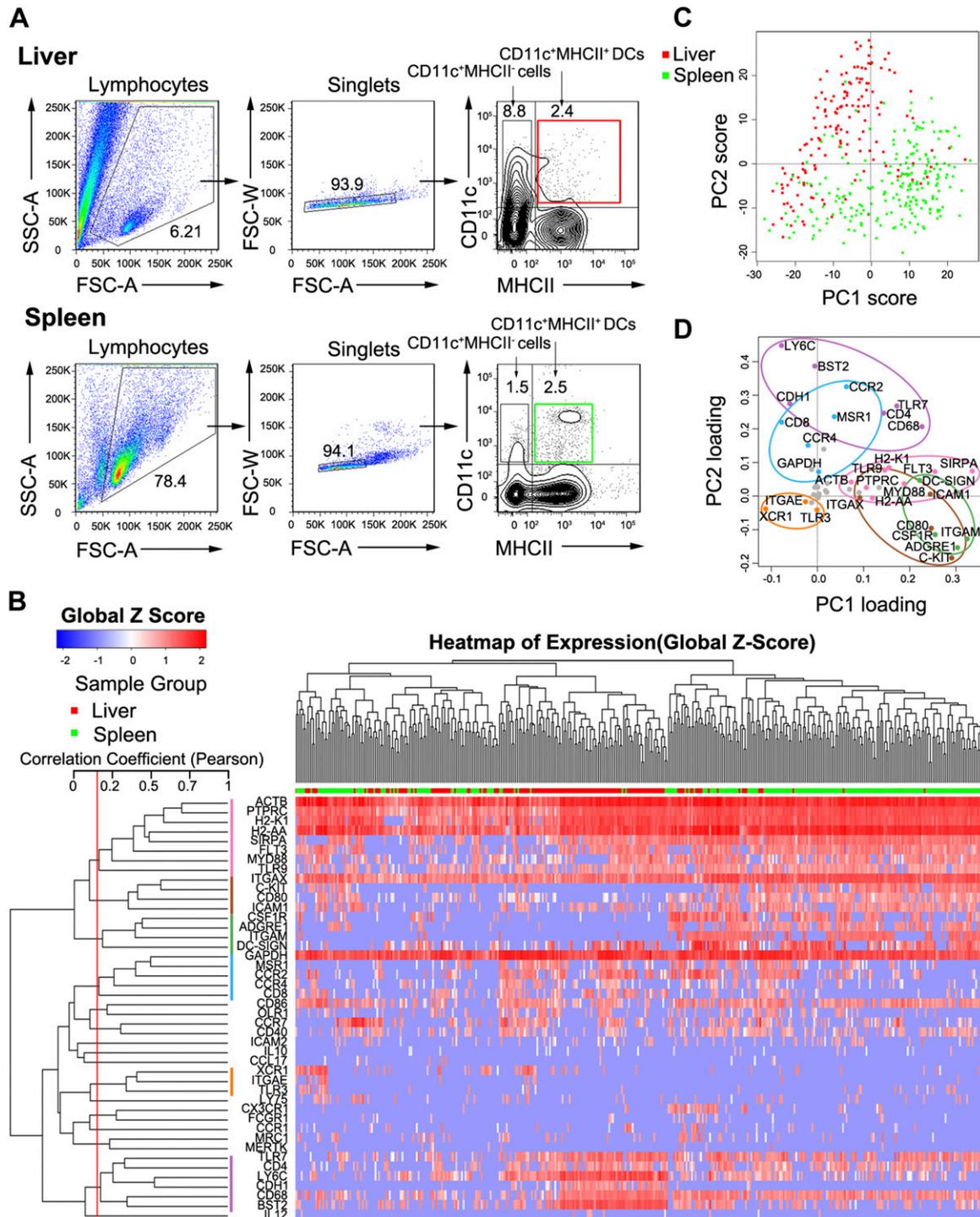
Figure 2. Single-cell gene expression analysis to distinguish the profiles of the DCs from the mouse liver and spleen. *A*) Gating strategy for sorting the single DCs from the mouse liver and spleen. First, live lymphocytes were segregated on FSC-A and SSC-A plots, and singlets from live lymphocytes were further gated by FSC-A and FSC-W. Then, liver CD11c⁺MHCII⁺ DCs (red box) and spleen CD11c⁺MHCII⁺ DCs (green box) were segregated from singlets on CD11c and MHCII plots, respectively. The percentages of CD11c⁺MHCII⁺ DCs in liver and spleen suspensions were calculated with the percentages of the 3 parts. *B*) The heat map revealed the expression levels of the 48 target genes from 151 single liver DCs (red square) and 229 single spleen DCs (green square). Each square in the heat map indicates the expression of the specific gene in the corresponding column from a specific single cell in the corresponding row. The genes were grouped into 6 gene clusters (correlation coefficient >0.15), which are marked with different colors (pink, brown, green, blue, orange, and purple). *C*) PCA of single DCs from the liver (red square) and spleen (green square). *D*) Gene loading for the PCA analysis; the genes are colored and circled according to the 6 clusters that were identified in the HC analysis depicted in *B*. The gray dots are unclustered genes.

CD11c$^+$MHCII$^+$ DCs in the liver was 0.12–0.16%. In the spleen cell suspensions, CD11c$^+$MHCII$^+$ DCs accounted for 1.58–1.89%.

The 336 single liver CD11c$^+$MHCII$^+$ DCs and the 304 single spleen CD11c$^+$MHCII$^+$ DCs from 6 individual mice were initially sorted by FACS. Then, the expression levels of the 48 target genes in each individual cell were quantified in parallel using 48.48 Dynamic Array chips with the Biomark system (Fluidigm). After genetic confirmation as LIN(CD3,CD19, NK1.1)$^-$CD45$^+$CD11c$^+$MHCII$^+$ cells, 154 liver DCs and 229 spleen DCs were identified and entered into the bioinformatic analysis.

Liver DCs and spleen DCs show different single-cell expression patterns

Based on the expression profiles of the 48 genes in the single DCs from liver and spleen, HC was applied (Fig. 2B). ITGAM was enriched in the spleen DCs, which suggested an accumulation of CD11b$^+$ DCs. LY6C and BST2 exhibited higher expression levels in the liver DCs, which revealed a higher percentage of pDCs.

PCA was also performed to reduce the dimensionality of the 48 gene expression profiles of single DCs. Using the first and second principal components (PC1 and PC2), the DCs from the liver and spleen were separated (Fig. 2C). Additionally, the contributions of each of the genes to PC1 and PC2 (termed the PC projections of the 48 genes) were identified. The genes were grouped into 6 gene clusters according to the HC analysis (Fig. 2D). For example, CSF1R, ADGRE1, ITGAM, and DC-SIGN were clustered together and primarily contributed to PC1, whereas genes such as LY6C, BST2, and CDH1 were clustered together and provided a major contribution to PC2.

This classification of the single DCs using HC and PCA reflects the divergence of the DCs in lymphoid and nonlymphoid tissues, which can be identified by changes in both phenotypic and functional markers.

Functional classification reveals functional heterogeneity of liver and spleen DCs

To illustrate the different expression patterns of the single DCs from the liver and spleen, a radar map was drawn to display the log$_2$-fold changes of the genes with significant P values (P < 0.05) (Fig. 3A and Supplemental Table S2). The results revealed that LY6C, BST2, CDH1, CCR2, and MSR1 were remarkably up-regulated in the liver DCs, whereas genes C-KIT, ADGRE1, CD80, ICAM1, and MYD88 were significantly enriched in the spleen DCs.

The single DCs were firstly subdivided using the classic phenotypic markers: conventional type 1 DCs (cDC1s), which are characterized by XCR1, ITGAE (CD103), and CD8; conventional type 2 DCs (cDC2s), which are identified by SIRPA (CD172), ITGAM (CD11b), CD4, and DC-SIGN; and pDCs, which can be recognized by LY6C and BST2 (31) (Fig. 3B). Violin plots revealed increased ratios of XCR1$^+$, ITGAE$^+$, and CD8$^+$ DCs in the liver and up-regulated ratios of SIRPA$^+$, ITGAM$^+$, CD4$^+$, and DC-SIGN$^+$

DCs in the spleen, with similar expression levels of positive groups. The ratios of LY6C$^+$ and BST2$^+$ DCs were increased in the liver as well as up-regulating expression levels. As a marker gene of epidermal LCs (32), CD207 (Langerin) was negatively expressed in the liver and spleen DCs.

In addition to classic phenotypic classification, our results also revealed a deep divergence of the single DCs based on a series of function-related markers (Fig. 3C). The expressions of 10 molecules in 7 functional groups was changed remarkably between the liver and the spleen DCs. CD80 was significantly up-regulated in the spleen DCs, suggesting a state of greater maturation in the spleen DCs. MYD88 was increased in the spleen DCs, which revealed an increased ability of the DCs in the spleen to activate CD4$^+$ T cells. TLR9 was elevated in the spleen DCs, which indicated increased pathogen recognition. MSR1 was enriched in the liver DCs, revealing greater lipid-uptake ability by the DCs from the liver. The remarkable accumulations of CCR1, CCR2, and CCR4 in the liver DCs may indicate enhanced migration properties of the DCs in the nonlymphoid tissues compared with the lymphoid tissues. Interestingly, CDH1 up-regulated in liver DCs, whereas ICAM1 was enriched in spleen DCs, which suggests that their adhesion ability may depend mainly on different adhesion molecules.

Moreover, the expression patterns of the DC definition-related markers provided further examples (Supplemental Fig. S2). The spleen DCs expressed greater levels of DC markers ITGAX (CD11c) and H2-AA (MHCII), which also indicated maturation of DCs (11). The increased level of C-KIT in the spleen DCs indicated that more DCs in the lymphoid organ expressed progenitor markers. We also analyzed several markers of macrophages: FCGR1 (CD64) and MERTK were rarely expressed in DCs and can thus be used as specific markers of macrophages. Although CD68 and ADGRE1 (F4/80) have also been reported to be markers of macrophages (33), our present research indicated that those 2 molecules were not specific and were also found on DCs.

These results suggested that single DCs reveal different phenotypic and functional classification in lymphoid and nonlymphoid tissue. Hence, this method was further examined in atherosclerosis, an immune-related disease.

Quantitatively increase of DCs in the atherosclerotic mouse model

Suspensions of mouse livers and spleens from healthy and atherosclerotic mice were subjected to flow cytometry (Fig. 4A, B), and the quantities and percentages of DCs, defined as CD11c$^+$MHCII$^+$, were analyzed (Fig. 4C, D). Compared with healthy liver DCs, the percentages of ApoE$^{-/-}$ liver DCs were significantly increased from 0.14–0.26% to 0.42–0.50%. The CD11c$^+$MHCII$^+$ DCs in the healthy spleen accounted for 1.98–2.32% of the cells, and that value increased to 3.45–4.07% in the ApoE$^{-/-}$ spleen. The remarkable recruitments of CD11c$^+$MHCII$^+$ DCs revealed the increased inflammatory responses in
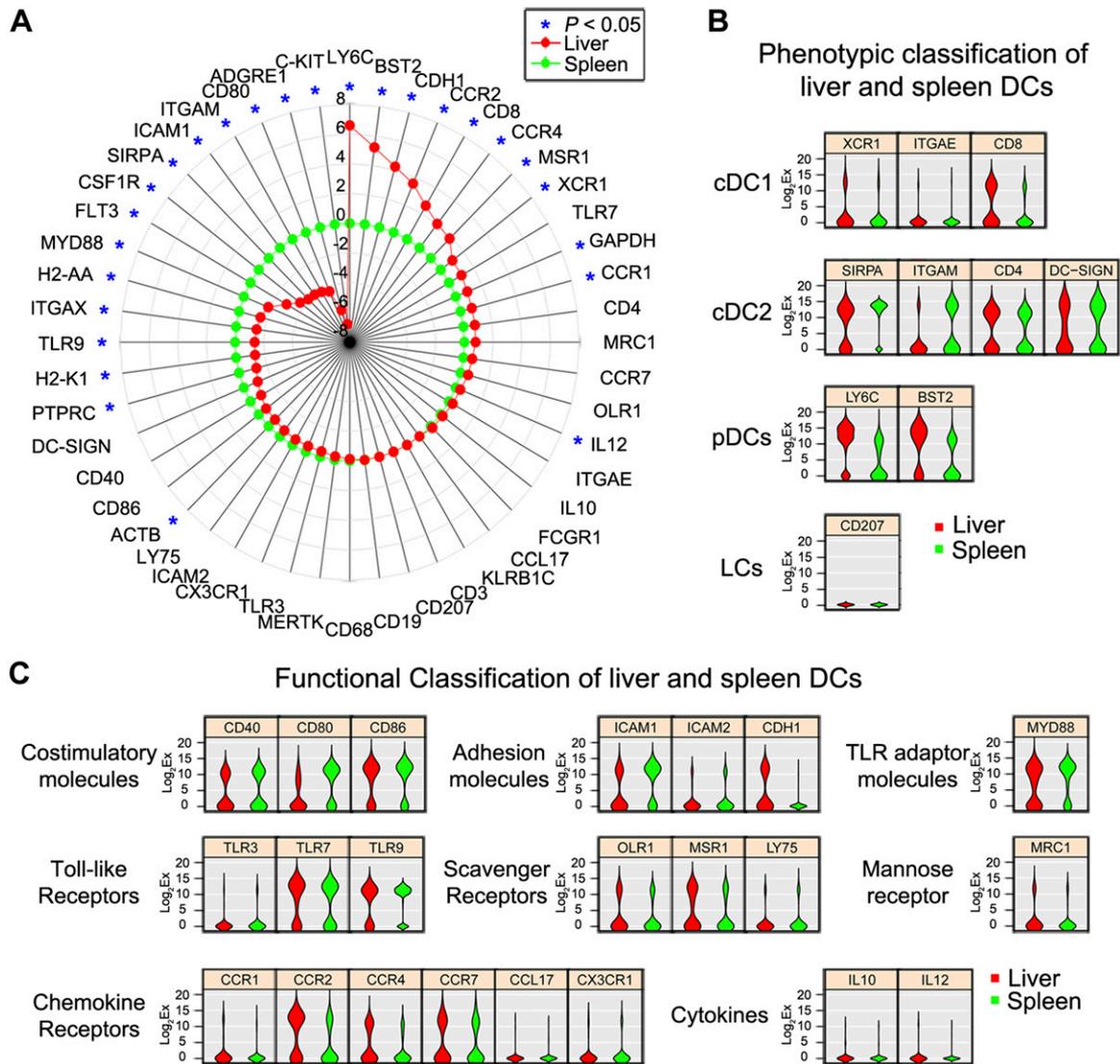
Figure 3. Phenotypic and functional classification of mouse liver and spleen DCs. *A*) The 48 genes are ordered in a clockwise manner with increasing $\log_2$-fold change. Each data point is the average expression level for a certain gene in the liver DCs (red points) and the spleen DCs (green points). $*P < 0.05$ by Student's *t* test. *B*) Violin plots showing the classifications of the liver DCs (red plots) and spleen DCs (green plots) with the reported phenotypic markers for cDC1, cDC2, pDC, and LCs. *C*) Classifications of the DCs from the liver (red plots) and spleen (green plots) based on 8 groups of function-related markers. See also Supplemental Fig. S2 and Supplemental Table S2.

both the lymphoid and nonlymphoid tissues during atherosclerosis.

DCs show distinct functional classification in the atherosclerotic mouse model

We proceeded to study the functional variations of the DCs between the healthy and $ApoE^{-/-}$ mouse model. Single DCs from healthy mouse livers ($n = 212$), single DCs from $ApoE^{-/-}$ mouse livers ($n = 206$), single DCs from healthy mouse spleens ($n = 224$), and single DCs from $ApoE^{-/-}$ mouse spleens ($n = 231$) were included in the analyses.

To probe the divergence of the expression patterns of the single DCs in the healthy and atherosclerotic mouse models, P values were calculated for the 48 target genes.

Supplemental Figure S3*A* lists all genes that changed significantly between the healthy and $ApoE^{-/-}$ liver DCs, including *CSF1R*, *ITGAM*, *CCR2*, and *CCR7*, and Supplemental Fig. S3*B* lists the genes that were markedly different between the healthy and $ApoE^{-/-}$ spleen DCs, such as *BST-2*, *CCR1*, *SIRPA*, and *ICAM1*.

Comparisons of the expression patterns of single DCs in liver and spleen from the healthy and $ApoE^{-/-}$ mice revealed variations in both phenotypic genes and functional genes (**Fig. 5*A*, *B*** and Supplemental Tables S3, 4). Regarding the phenotypic markers, *ITGAM* and *DC-SIGN* were enriched in the $ApoE^{-/-}$ liver DCs, which indicated increased rates of cDC2. *LY6C* and *BST2* accumulation in the $ApoE^{-/-}$ spleen DCs suggested an increased proportion of pDCs. Differently expressed functional markers and their potential roles were also demonstrated (Fig. 5*C*). The expression of the TLR genes *TLR7* and *TLR9* was
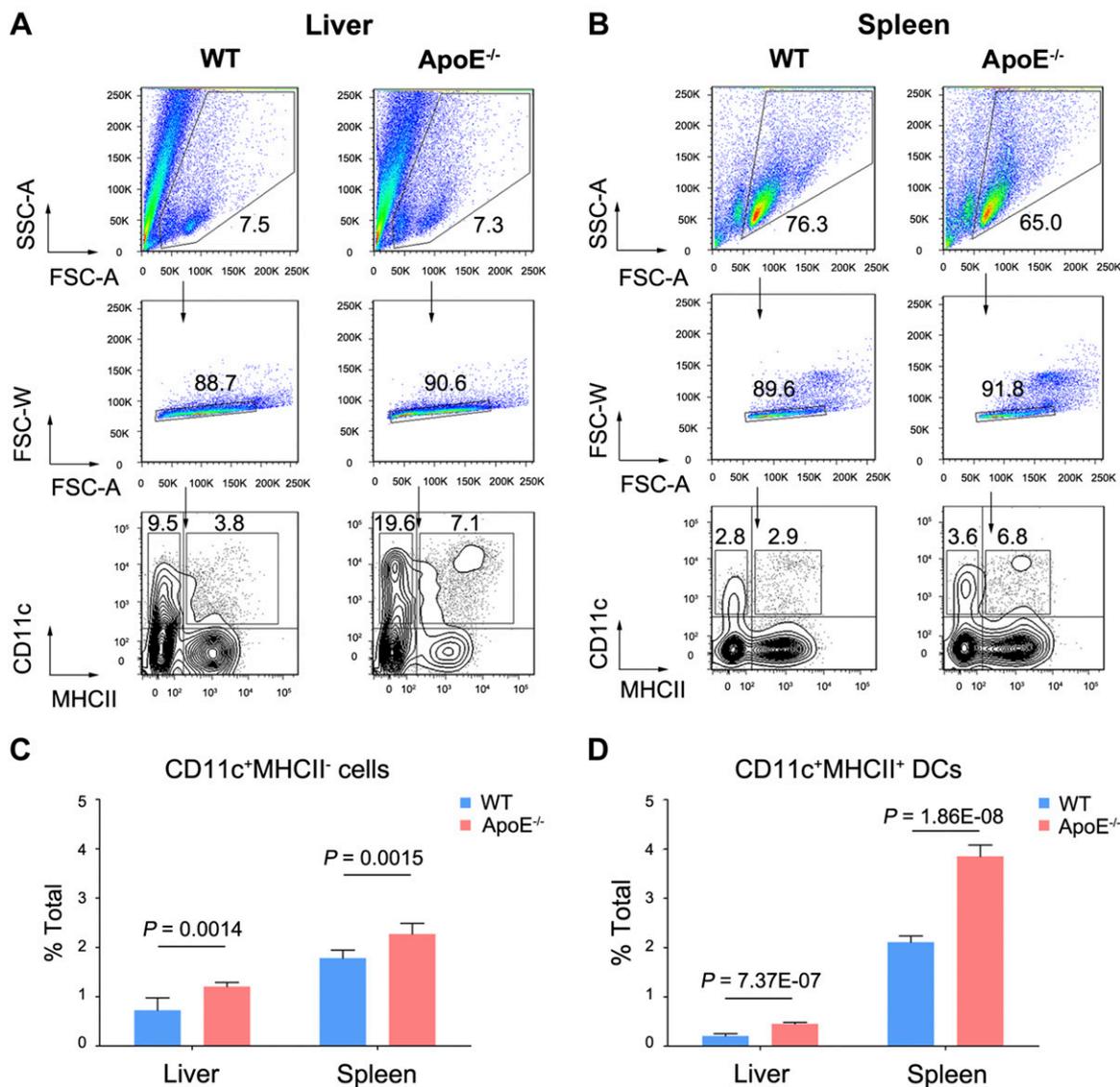
Figure 4. Accumulation of DCs in mouse liver and spleen from the atherosclerotic mouse model. *A, B*) FACS plots for the identifications of the CD11c⁺MHCII⁻ cells and CD11c⁺MHCII⁺ DCs in the liver (*A*) and spleen (*B*) from the healthy and atherosclerotic mice. *C, D*) Percentages of CD11c⁺MHCII⁻ cells (*C*) and CD11c⁺MHCII⁺ DCs (*D*) from the wild-type (WT; blue) and $ApoE^{-/-}$ (red) mice. The data are represented as the means ± sd. Each figure represents 6 experiments.

significantly increased in the $ApoE^{-/-}$ spleen DCs, which indicated elevated innate responses. *MYD88* was markedly up-regulated in the $ApoE^{-/-}$ liver DCs, which indicated increased T-cell stimulation. *OLR1* was significantly increased in the $ApoE^{-/-}$ liver DCs, and that increase might lead to enhanced oxLDL-induced DC activation. Regarding the chemokine receptors, *CCR2* and *CX3CR1* were elevated in the $ApoE^{-/-}$ liver DCs, and *CCR1* was up-regulated in the $ApoE^{-/-}$ spleen DCs, which may be suggestive of increased migration and T-cell–recruitment abilities. Interestingly, *CCR7* was down-regulated in the $ApoE^{-/-}$ liver DCs. Regarding adhesion genes, the expression of the *CDH1* and *ICAM1* genes was decreased in the $ApoE^{-/-}$ liver and spleen DCs, respectively, and *ICAM2* was increased in the $ApoE^{-/-}$ spleen; those differences might contribute to the different adhesion properties of the DCs. Additionally, *CD40* was up-regulated in the $ApoE^{-/-}$ liver DCs, whereas *CD80* was down-regulated in the $ApoE^{-/-}$ spleen DCs; that

difference is reflective of the heterogeneity of the costimulatory molecules.

Our approach of using single-cell analysis revealed the heterogeneity of function-related markers under inflammatory conditions.

Migration-related DC molecule CCR7 in atherogenesis

To confirm the changes revealed by the gene profiling based on phenotypic and functional markers, the migration-related molecule CCR7 was detected by immunofluorescence in the liver and spleen DCs from the healthy and atherosclerotic mice (**Fig. 6***A–D*). Liver DCs (CD11c⁺) were mostly found in the periportal area, and spleen DCs (CD11c⁺) were distributed in the parenchyma. Consistent with the previous analysis, more DCs (CD11c⁺) were found in the livers and spleens of the $ApoE^{-/-}$ mice. The expression of
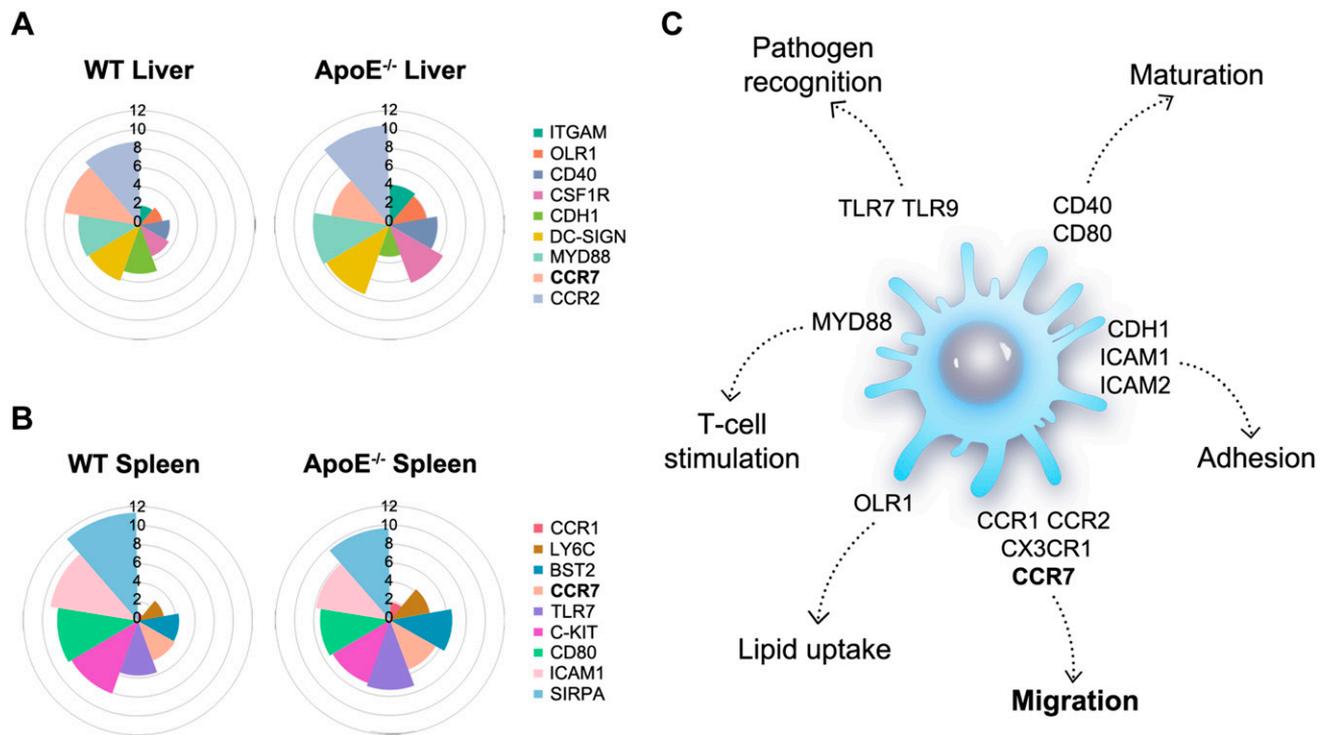
Figure 5. DCs in the healthy and $ApoE^{-/-}$ mice showed different gene expression patterns. *A*, *B*) Wind rose maps show the different expression patterns of the DCs in the liver (*A*) and spleen (*B*) from the wild-type (WT) and $ApoE^{-/-}$ mice with the average Log$_2$Ex values. The genes that exhibited large differences in the Log$_2$Ex values (>1) are displayed. *C*) Diagram of differentially expressed genes of the DCs and their potential roles in atherosclerosis. Each figure represents 6 experiments. *CCR7*, which is marked in bold, was the migration-related molecule used in the subsequent portion of the study. See also Supplemental Fig. S3 and Supplemental Tables S3, S4.

CCR7 was slightly up-regulated in the $ApoE^{-/-}$ spleen DCs, and the DCs (CD11c$^+$) in atherosclerotic livers exhibited a down-regulation of CCR7 at the single-cell level.

Next, the distributions of DCs (CD11c$^+$) and the expression of CCR7 in healthy and atherosclerotic aorta were compared (Fig. 6*E*, *F*). We observed a subendothelial location of DCs in the healthy aorta, and the DCs dramatically accumulated in atherosclerotic plaques. Additionally, there was an up-regulation of CCR7 in the DCs of atherosclerotic aorta, which was thought to mediate DC egress during lesion regression (34).

DISCUSSION

The rarity of DCs in tissues has made it rather difficult to explore their heterogeneity. *In vitro* study by culturing DCs cannot reflect the real biology (35), and bulk cell analysis may mask DC heterogeneity (36). Limited by detection methods, prior studies used only a few phenotypic markers to divide DCs at 1 time (24). Recently, mass cytometry, based on 14 markers, was used to analyze DC populations across tissues and species (2). In the present analysis, we simultaneously analyzed 46 phenotypic and functional markers, which revealed a similar DC heterogeneity to previous flow cytometry results (2). For example, *XCR1*, the marker of cDC1, accounted for 21.4% in liver DCs and 13.1% in spleen DCs, whereas the ratio of *SIRPA*, the marker of cDC2, was 61.7% in liver DCs and 86.0% in spleen DCs.

Furthermore, our work also contributes to an understanding of functional DC heterogeneity, which has never been used for DC classification before. We showed distinct expression patterns of functional markers in lymphoid and nonlymphoid DCs, suggesting their potential roles in migration, maturation, and T-cell stimulation. Chemokine receptors *CCR1*, *CCR2*, and *CCR4* were up-regulated in liver DCs, suggesting enhanced migration ability. Previous studies were mainly focused on *CCR7* (37), which may not be sufficient to understand DC migration in nonlymphoid tissues. Spleen DCs exhibited a more-mature state with an enriched costimulatory molecule *CD80* (16), which corresponded to our immunofluorescence showing more dendrites. DCs were close to the T-cell zone in the spleen. Up-regulation of the TLR adaptor *MYD88* in spleen DCs indicated enhanced T-cell activation (15), which may be related with DC–T cell interactions.

Previous research revealed that DCs accumulate in atherosclerotic lesions (38) and are predisposed to atherosclerosis, which is a well-known, chronic inflammatory disease of the large and medium arteries (39). We then concentrated on the migration ability of DCs in $ApoE^{-/-}$ mice and demonstrated an unexpected change in DCs, which could be hidden by traditional bulk-cell analysis. Our results showed an increase in *CCR7* in spleen DCs in the $ApoE^{-/-}$ mice. Interestingly, *CCR7* was decreased in single DCs from the $ApoE^{-/-}$ liver. *CCR7* was reported to participate in the egress of DCs. In the atherosclerosis regression model, blockade of CCR7 ligands CCL19 and CCL21 preserved CD11c$^+$ cells in atherosclerotic plaques,
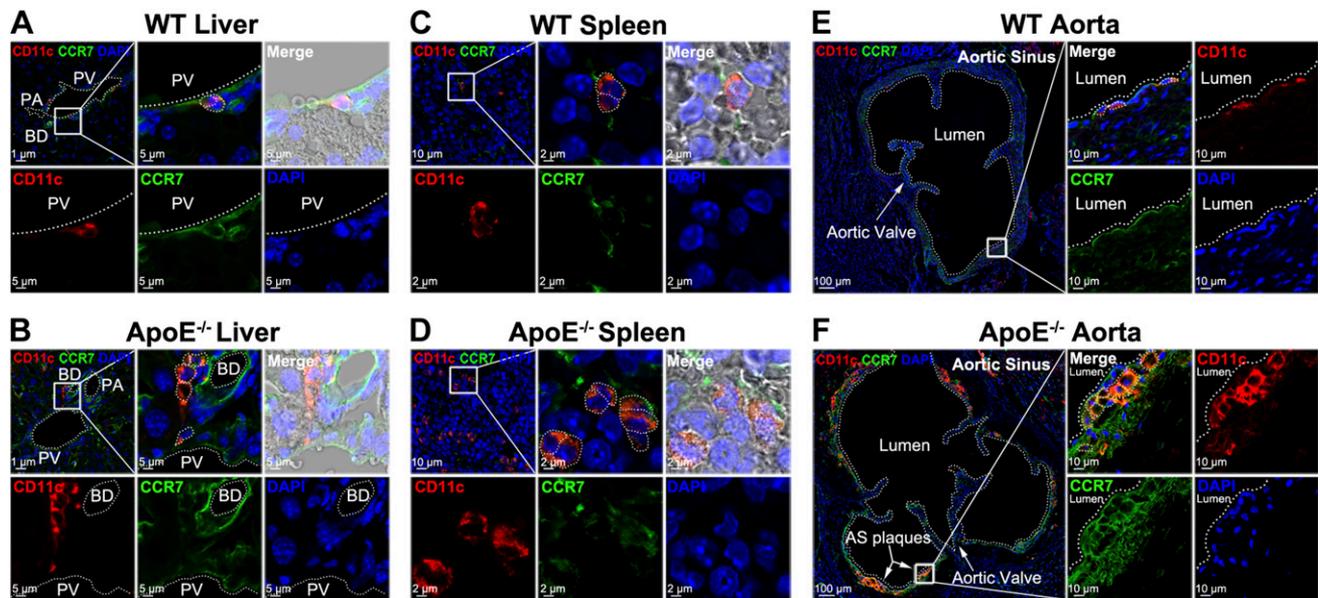
Figure 6. CCR7 expression in the healthy and *ApoE*$^{-/-}$ mice. Costaining for CD11c (red), CCR7 (green), and DAPI (blue) in the liver, spleen, and aorta root sections from the wild-type (WT) and *ApoE*$^{-/-}$ mice. *A, B*) Upper left image shows the periportal area; dotted line demarcates PV, PA, and BD. Scale bar, 1 μm. The following images show higher magnification; dotted circles demarcate CD11c$^+$ cells. Scale bar, 5 μm. PV, portal venule; PA, portal arteriole; BD, bile duct. *C, D*) Upper left image shows the parenchyma of the spleen. Scale bar, 10 μm. The following images show higher magnification; dotted circles demarcate CD11c$^+$ cells. Scale bar, 2 μm. *E, F*) Left image shows the aortic sinus (dotted line). Scale bar, 100 μm. The following images show higher magnification; dotted circles demarcate CD11c$^+$ cells. Scale bar, 10 μm. Aortic valves and atherosclerotic plaques are pointed out with arrowheads.

suggesting a CCR7-dependent emigration for DCs (34). Decreased expression of *CCR7* in *ApoE*$^{-/-}$ liver DCs may indicate impaired migration under sustained hyperlipidemia conditions, which remains to be explained.

Additionally, the present phenotypic and functional classifications have been focused on commonly defined DCs, that is, CD11c$^+$MHCII$^+$, whereas flow cytometry also identified another subgroup of cells, characterized as CD11c$^+$MHCII$^-$, which are considered to be DC precursors in mice (40, 41). The percentages of CD11c$^+$MHCII$^-$ cells were significantly up-regulated from 0.42–1.17% in the healthy liver to 1.08–1.30% in the *ApoE*$^{-/-}$ liver, and the ratios were increased from 1.58–1.95% in the healthy spleen to 1.96–2.60% in the *ApoE*$^{-/-}$ spleen. The up-regulation of the DC precursor CD11c$^+$MHCII$^-$ cells indicated a possible source of the recruited CD11c$^+$MHCII$^+$ DCs in the liver and spleen. The heterogeneity and functions of this specific population of DCs still need further explorations.

Although compared with single-cell RNA sequencing (scRNA-seq), sc-qPCR has its limitation on throughput, sc-qPCR has the strengths of lower cost, faster data processing, less-redundant information, and easier commercialization (42, 43). In addition, neither sample library preparation nor deep sequencing was needed to perform sc-qPCR, which are the key steps for scRNA-seq and require more-expensive reagents and longer workflow periods. scRNA-seq also requires more-complex bioinformatic techniques for handling redundant information, which increases the difficulties of data analysis and extends the experimental duration. As a "targeted" technology, sc-qPCR can be performed with a preselected and specific set of gene primers, which may be automated and commercialized for potential clinical application. In addition, scRNA-seq still has limitations in detecting specific, low-abundance transcripts, which may be crucial for finding new subsets (44), by hiding them under the high technical noise. Our study showed the applications of sc-qPCR on exploration of not only phenotypic but also functional heterogeneity of DCs in the steady state and in inflammatory disease. Furthermore, this method may provide new insights into the participation of DCs in inflammatory diseases, disease pathogeneses, and associated molecular mechanisms. **Fj**

AUTHOR CONTRIBUTIONS

Q. Shi and Y.-X. Qi designed the research; Q. Shi, F. Zhuang, J.-T. Liu, N. Li, Y.-X. Chen, Q.-P. Yao, Y. Han, and S.-S. Li performed the research; Q. Shi, X.-B. Su, and A.-H. Yao analyzed the data; and Q. Shi, Y.-X. Qi, and Z.-L. Jiang wrote the manuscript.

REFERENCES

1. Steinman, R. M., Adams, J. C., and Cohn, Z. A. (1975) Identification of a novel cell type in peripheral lymphoid organs of mice. IV. Identification and distribution in mouse spleen. *J. Exp. Med.* **141**, 804–820

2. Guilliams, M., Dutertre, C. A., Scott, C. L., McGovern, N., Sichien, D., Chakarov, S., Van Gassen, S., Chen, J., Poidinger, M., De Prijck, S., Tavernier, S. J., Low, I., Irac, S. E., Mattar, C. N., Sumatoh, H. R., Low, G. H. L., Chung, T. J. K., Chan, D. K. H., Tan, K. K., Hon, T. L. K., Fossum, E., Bogen, B., Choolani, M., Chan, J. K. Y., Larbi, A., Luche, H., Henri, S., Saeys, Y., Newell, E. W., Lambrecht, B. N., Malissen, B., and Ginhoux, F. (2016) Unsupervised high-dimensional analysis aligns dendritic cells across tissues and species. *Immunity* **45**, 669–684

3. Choi, J. H., Do, Y., Cheong, C., Koh, H., Boscardin, S. B., Oh, Y. S., Bozzacco, L., Trumpfheller, C., Park, C. G., and Steinman, R. M. (2009) Identification of antigen-presenting dendritic cells in mouse aorta and cardiac valves. *J. Exp. Med.* **206**, 497–505

4. Banchereau, J., and Steinman, R. M. (1998) Dendritic cells and the control of immunity. *Nature* **392**, 245–252

5. Murphy, T. L., Grajales-Reyes, G. E., Wu, X., Tussiwand, R., Briseño, C. G., Iwata, A., Kretzer, N. M., Durai, V., and Murphy, K. M. (2016) Transcriptional control of dendritic cell development. *Annu. Rev. Immunol.* **34**, 93–119

6. Geissmann, F., Manz, M. G., Jung, S., Sieweke, M. H., Merad, M., and Ley, K. (2010) Development of monocytes, macrophages, and dendritic cells. *Science* **327**, 656–661

7. Sponaas, A. M., Cadman, E. T., Voisine, C., Harrison, V., Boonstra, A., O'Garra, A., and Langhorne, J. (2006) Malaria infection changes the ability of splenic dendritic cell populations to stimulate antigen-specific T cells. *J. Exp. Med.* **203**, 1427–1433

8. Plantinga, M., Guilliams, M., Vanheerswynghels, M., Deswarte, K., Branco-Madeira, F., Toussaint, W., Vanhoutte, L., Neyt, K., Killeen, N., Malissen, B., Hammad, H., and Lambrecht, B. N. (2013) Conventional and monocyte-derived CD11b+ dendritic cells initiate and maintain T helper 2 cell-mediated immunity to house dust mite allergen. *Immunity* **38**, 322–335

9. Muzaki, A. R. B. M., Tetlak, P., Sheng, J., Loh, S. C., Setiagani, Y. A., Poidinger, M., Zolezzi, F., Karjalainen, K., and Ruedl, C. (2016) Intestinal CD103+CD11b− dendritic cells restrain colitis via IFN-γ–induced anti-inflammatory response in epithelial cells. *Mucosal Immunol.* **9**, 336–351

10. Segura, E., and Amigorena, S. (2013) Inflammatory dendritic cells in mice and humans. *Trends Immunol.* **34**, 440–445

11. Lutz, M. B., and Schuler, G. (2002) Immature, semi-mature and fully mature dendritic cells: which signals induce tolerance or immunity? *Trends Immunol.* **23**, 445–449

12. Durai, V., and Murphy, K. M. (2016) Functions of murine dendritic cells. *Immunity* **45**, 719–736

13. Wang, D., Sun, B., Feng, M., Feng, H., Gong, W., Liu, Q., and Ge, S. (2015) Role of scavenger receptors in dendritic cell function. *Hum. Immunol.* **76**, 442–446

14. Comrie, W. A., Li, S., Boyle, S., and Burkhardt, J. K. (2015) The dendritic cell cytoskeleton promotes T cell adhesion and activation by constraining ICAM-1 mobility. *J. Cell Biol.* **208**, 457–473

15. Gelman, A. E., LaRosa, D. F., Zhang, J., Walsh, P. T., Choi, Y., Sunyer, J. O., and Turka, L. A. (2006) The adaptor molecule MyD88 activates PI-3 kinase signaling in CD4+ T cells and enables CpG oligodeoxynucleotide-mediated costimulation. *Immunity* **25**, 783–793

16. Steinman, R. M., and Idoyaga, J. (2010) Features of the dendritic cell lineage. *Immunol. Rev.* **234**, 5–17

17. Shortman, K., and Naik, S. H. (2007) Steady-state and inflammatory dendritic-cell development. *Nat. Rev. Immunol.* **7**, 19–30

18. Nickel, T., Schmauss, D., Hanssen, H., Sicic, Z., Krebs, B., Jankl, S., Summo, C., Fraunberger, P., Walli, A. K., Pfeiler, S., and Weis, M. (2009) oxLDL uptake by dendritic cells induces upregulation of scavenger-receptors, maturation and differentiation. *Atherosclerosis* **205**, 442–450

19. Fukata, M., Breglio, K., Chen, A., Vamadevan, A. S., Goo, T., Hsu, D., Conduah, D., Xu, R., and Abreu, M. T. (2008) The myeloid differentiation factor 88 (MyD88) is required for CD4+ T cell effector function in a murine model of inflammatory bowel disease. *J. Immunol.* **180**, 1886–1894

20. Chea, S., Schmutz, S., Berthault, C., Perchet, T., Petit, M., Burlen-Defranoux, O., Goldrath, A. W., Rodewald, H. R., Cumano, A., and Golub, R. (2016) Single-cell gene expression analyses reveal heterogeneous responsiveness of fetal innate lymphoid progenitors to notch signaling. *Cell Rep.* **14**, 1500–1516

21. Jaitin, D. A., Kenigsberg, E., Keren-Shaul, H., Elefant, N., Paul, F., Zaretsky, I., Mildner, A., Cohen, N., Jung, S., Tanay, A., and Amit, I. (2014) Massively parallel single-cell RNA-seq for marker-free decomposition of tissues into cell types. *Science* **343**, 776–779

22. National Research Council. (2010) *Guide for the Care and Use of Laboratory Animals*, National Academies Press, Washington, DC, USA

23. Ginhoux, F., Liu, K., Helft, J., Bogunovic, M., Greter, M., Hashimoto, D., Price, J., Yin, N., Bromberg, J., Lira, S. A., Stanley, E. R., Nussenzweig, M., and Merad, M. (2009) The origin and development of nonlymphoid tissue CD103+ DCs. *J. Exp. Med.* **206**, 3115–3130

24. Merad, M., Sathe, P., Helft, J., Miller, J., and Mortha, A. (2013) The dendritic cell lineage: ontogeny and function of dendritic cells and their subsets in the steady state and the inflamed setting. *Annu. Rev. Immunol.* **31**, 563–604

25. Murtagh, F., and Contreras, P. (2012) Algorithms for hierarchical clustering: an overview. *Wiley Interdiscip. Rev. Data Min. Knowl. Discov.* **2**, 86–97

26. Schraml, B. U., and Reis e Sousa, C. (2015) Defining dendritic cells. *Curr. Opin. Immunol.* **32**, 13–20

27. Blasius, A. L., and Beutler, B. (2010) Intracellular Toll-like receptors. *Immunity* **32**, 305–315

28. Emara, M., Royer, P. J., Abbas, Z., Sewell, H. F., Mohamed, G. G., Singh, S., Peel, S., Fox, J., Shakib, F., Martinez-Pomares, L., and Ghaemmaghami, A. M. (2011) Recognition of the major cat allergen Fel d 1 through the cysteine-rich domain of the mannose receptor determines its allergenicity. *J. Biol. Chem.* **286**, 13033–13040

29. Ma, X., Yan, W., Zheng, H., Du, Q., Zhang, L., Ban, Y., Li, N., and Wei, F. (2015) Regulation of IL-10 and IL-12 production and function in macrophages and dendritic cells [eCollection]. *F1000 Res.* **4**

30. Poltorak, M. P., and Schraml, B. U. (2015) Fate mapping of dendritic cells. *Front. Immunol.* **6**, 199

31. Mildner, A., and Jung, S. (2014) Development and function of dendritic cell subsets. *Immunity* **40**, 642–656

32. Schuler, G., Romani, N., and Steinman, R. M. (1985) A comparison of murine epidermal Langerhans cells with spleen dendritic cells. *J. Invest. Dermatol.* **85** (1 Suppl), 99s–106s

33. Zhang, X., Goncalves, R., and Mosser, D. M. (2008) The isolation and characterization of murine macrophages. *Curr. Protoc. Immunol.* **Chapter 14**, Unit 14.1–

34. Trogan, E., Feig, J. E., Dogan, S., Rothblat, G. H., Angeli, V., Tacke, F., Randolph, G. J., and Fisher, E. A. (2006) Gene expression changes in foam cells and the role of chemokine receptor CCR7 during atherosclerosis regression in ApoE-deficient mice. *Proc. Natl. Acad. Sci. USA* **103**, 3781–3786

35. Helft, J., Böttcher, J., Chakravarty, P., Zelenay, S., Huotari, J., Schraml, B. U., Goubau, D., and Reis e Sousa, C. (2015) GM-CSF mouse bone marrow cultures comprise a heterogeneous population of CD11c+MHCII+ macrophages and dendritic cells. *Immunity* **42**, 1197–1211

36. Shapiro, E., Biezuner, T., and Linnarsson, S. (2013) Single-cell sequencing-based technologies will revolutionize whole-organism science. *Nat. Rev. Genet.* **14**, 618–630

37. Randolph, G. J., Ochando, J., and Partida-Sánchez, S. (2008) Migration of dendritic cell subsets and their precursors. *Annu. Rev. Immunol.* **26**, 293–316

38. Busch, M., Westhofen, T. C., Koch, M., Lutz, M. B., and Zernecke, A. (2014) Dendritic cell subset distributions in the aorta in healthy and atherosclerotic mice. *PLoS One* **9**, e88452

39. Jongstra-Bilen, J., Haidari, M., Zhu, S. N., Chen, M., Guha, D., and Cybulsky, M. I. (2006) Low-grade chronic inflammation in regions of the normal mouse arterial intima predisposed to atherosclerosis. *J. Exp. Med.* **203**, 2073–2083

40. Del Hoyo, G. M., Martín, P., Vargas, H. H., Ruiz, S., Arias, C. F., and Ardavín, C. (2002) Characterization of a common precursor population for dendritic cells. *Nature* **415**, 1043–1047

41. Liu, K., Victora, G. D., Schwickert, T. A., Guermonprez, P., Meredith, M. M., Yao, K., Chu, F. F., Randolph, G. J., Rudensky, A. Y., and Nussenzweig, M. (2009) *In vivo* analysis of dendritic cell development and homeostasis. *Science* **324**, 392–397

42. Papalexi, E., and Satija, R. (2018) Single-cell RNA sequencing to explore immune cell heterogeneity. *Nat. Rev. Immunol.* **18**, 35–45

43. Kolodziejczyk, A. A., Kim, J. K., Svensson, V., Marioni, J. C., and Teichmann, S. A. (2015) The technology and biology of single-cell RNA sequencing. *Mol. Cell* **58**, 610–620

44. Saliba, A. E., Westermann, A. J., Gorski, S. A., and Vogel, J. (2014) Single-cell RNA-seq: advances and future challenges. *Nucleic Acids Res.* **42**, 8845–8860